PCCP

ROYAL SOCIETY OF CHEMISTRY

PAPER

View Article Online
View Journal | View Issue

Cite this: *Phys. Chem. Chem. Phys.*, 2022, **24**, 11552

Probing the mechanisms of enhanced crystallisation of APS in the presence of ultrasound†

Peter R. Birkin, *[a] Jack J. Youngs,[a] Tadd T. Truscott[b] and Silvana Martini[c]

Understanding the origins of the enhancement of crystallisation of a lipid (all-purpose shortening, APS) through the application of ultrasound is a fundamental pre-requisite for the exploitation of this technique in a wider context. To this end, we show here a number of measurements designed to probe the mechanisms responsible for this effect. For example, we show how the type of bubble cluster, produced at the sound source, alters the bubble population and residency time. In addition, to probe the various contributions to the enhanced crystallisation rate, isolation of the cluster environment below the piston like emitter (PLE) used as the ultrasonic source was shown to reduce the enhancement observed, but did not remove it entirely. This implied that the exposure of the liquid to pressure shocks and the environment around the cluster has a positive effect on the crystallisation kinetics. In turn the addition of extra seed crystals and mechanical agitation also enhances the rate of crystallisation. Finally, the time at which ultrasonic irradiation of the fluid is applied is shown to alter the kinetics observed. These observations suggest that two components are important: large bubble populations and mechanical effects on pre-existing crystals. These findings suggest that maximising these effects could be an eloquent way to enhance and control the material characteristics of materials produced in this manner.

Received 14th December 2021,
Accepted 1st March 2022

DOI: 10.1039/d1cp05701d

rsc.li/pccp

Introduction

The effects of cavitation on the physical and chemical properties of a system are often complex with many different factors to consider. For example, chemical processes can be affected through the sonochemical hotspot,[1–3] surface activation or even mechanochemical effects.[4] Physical processes can be equally dramatic with the generation of intense shockwaves, the erosion of surfaces,[5] shear driven processes, bubble oscillation[6,7] with associated forced convection (sometimes referred to as microstreaming[7,8]) and the emission of short duration light flashes[9,10] noted. These complexities have been investigated with a multidisciplinary approach. However, many of these investigations have centred on aqueous environments. While many non-aqueous environment studies are noteworthy, this area is perhaps less well understood. In this context, lipid systems have received some attention.[11–13] While general lipid chemistry is of interest, food lipids are particularly interesting as they make a considerable contribution to the global food industry.[14] One such area of interest has been reports of the effects of cavitation on the solidification of lipids. In this case, high-intensity ultrasound, or HIU, can be shown to have beneficial effects in terms of the acceleration of the crystallisation kinetics as well as alteration of the material characteristics of the resultant solid. The root of the effect has often been attributed to cavitation. While this may be true, considering the complex environment, from a chemical and physical perspective, much more work is required to unravel the exact cause of the changes observed. This is not only illustrative from an academic perspective, but the understanding gathered by these studies will have many potential applications. For example, rather than the *ad hoc* application of sound energy at a particular frequency in a wide range of cell configurations, understanding what effect is necessary will mean that the approach can be tailored so that the positive effects are maximised while the negative effects (*e.g.*, the oxidation[15] of the chemical species within the media) are minimised. To gather the information necessary, an array of experimental techniques is desirable. These techniques must have a number of characteristics including the temporal resolution, the sensitivity,

[a] *Department of Chemistry, University of Southampton, Southampton, UK, SO17 1BJ, UK. E-mail: prb2@soton.ac.uk*
[b] *Department of Mechanical and Aerospace Engineering, Utah State University, Logan, UT, 84322-4130, USA*
[c] *Department of Nutrition, Dietetics, and Food Sciences, Utah State University, Logan, UT, 84322-8700, USA*

† Electronic supplementary information (ESI) available. See DOI: https://doi.org/10.1039/d1cp05701d

and the ability to operate with an analytical basis in lipid systems exposed to HIU. Techniques such as high-speed imaging, light scattering[16] (both *in situ* and of the resultant material), acoustic measurements, thermal profiling[16] and characterisation of the resultant materials can be highly rewarding in this context. For example, these approaches have been used with food oils and indicated a rich and interesting set of conditions are present. This includes cluster dynamics, high-speed streamers, bifurcated streamers, local heating and altered crystallisation kinetics (and material changes) related to the dynamics of the bubbles present. Central to this is the cluster that forms at the eroded tip deployed in the media. This fascinating phenomenon appears to be related to the effects observed.

While much progress has been made, several key questions remain. First, why does cavitation generated in this manner alter the kinetics of crystallisation so effectively? Second, what are the root causes of this alteration? Third, why does the particular cluster present give rise to varying degrees of effect observed? Some insight into the answers to these questions will now be given using experimental observations related to the lifetime of bubbles within the media and the effect of different treatment protocols on the crystallisation kinetics.

Methods

Materials

Experiments were performed using sunflower oil (SFO) in the isolation cell and all-purpose shortening (APS, Bunge). Acrylic (ACR) cells were obtained from Striking Displays and ABS from Verbatim.

Crystallisation experiments

APS samples were melted in a microwave oven and then stored in an oven at 80 °C for 30 minutes to remove residual crystal memory. The melted sample (100 g) was transferred to a double-walled thermostatic crystallisation cell connected to an external water bath (Grant, LT ecocool 100), set to the relevant crystallisation temperature (T_c). The cooling regime is shown in Fig. S1 (ESI†) for reference. To measure the crystallisation kinetics, samples were transferred to p-NMR tubes, previously pre-heated to the crystallisation temperature. The solid fat content (SFC) of the samples was then monitored by recording the SFC *vs.* time using NMR Minispec mq20 series (Bruker, California, USA). The data was fitted to the Gompertz model[17] (see ref. 18 for further details).

Optical sensor construction calibration and operation

The construction and calibration of the optical transmission sensor (OTS) has been described previously.[19] In brief this sensor was fabricated using a glass capillary (1.6 mm internal diameter). A photodiode and LED were used as the detector and emitter respectively. These were placed on opposite sides of the glass capillary set in Epofix resin (Struers) and polished down to reveal a channel. A simple amplifier[16] (gain 10^6) was used to detect the signal from the photodiode which was recorded on a DAQ system (USB204, Measurement computing). To draw fluid containing the generated bubbles through the OTS, a pressure rig was deployed were a gas syringe (120 ml, Rapid Electronics) and mass was used to generate a constant reduced pressure compared to the atmospheric pressure.[20] The exact pressure difference was monitored using an EBRO vacuum meter (VM 2000) and is reported in each figure legend as appropriate. The data was captured using software written in VB2010 incorporating Measurement studio (National Instruments). Data analysis (*e.g.*, for peak finding) was undertaken using Matlab.

HIU setup

Cavitation was generated using a 'piston like emitter' (PLE, Misonix, S3000, f = 20 kHz) immersed in the relevant media here an oil (SFO or APS). A 3.2 mm diameter eroded[16] tip was employed in all cases. The tip of the PLE was not polished as this was found not to be conducive to the formation of stable clusters in these oil systems (see ref. 16). The cluster characteristics have been detailed before and are generated at a set power level.[18] These clusters are denoted by f/N where f is the PLE frequency and N an integer value.[16] The OTS was positioned with respect to the PLE tip using micrometers and stages (Thor labs).

Crystal microstructure

A polarised light microscope (PLM-Olympus BX 41, Tokyo, Japan) fitted with a digital camera (Infinity 2, Lumenera Scientific, Ottawa, Canada) was used to record the crystal microstructure of crystallised lipid material. Images were recorded approximately 20 minutes after initial sample cooling.

Viscoelastic properties

A magnetic bearing rheometer (model AR-G2, TA Instruments, New Castle, DE, USA) was used to measure the elasticity of crystallised samples after approximately 60 minutes of crystallisation. A parallel plate geometry (40 mm diameter) was employed and maintained at the relevant T_c (26 °C or 30 °C). Depending upon the relative hardness of the sample, a gap of between 500–1000 μm was used. Oscillatory tests were performed by a strain sweep step from 0.0008–10% of strain and equilibration time of 1 minute. Viscoelastic parameters such as the storage modulus (G') were recorded at 0.01% of strain.

Hardness

The hardness of the crystallised material was evaluated by texture profile analysis (TPA) using a Texture Analyser (model TA, XT Plus, Texture Technologies Corp., Scarsdale, NY, USA). Samples were transferred to labelled plastic tubes (1 cm diameter) after 60 minutes and stored at 5 °C for 48 h. Chilled samples were cut to a height of approximately 1 cm, placed on the sample platform and a two-step compression with a 5 cm diameter cylindrical probe performed. A constant speed of 5 mm s^{-1} and compression strain of 25% were employed. Note, data was not recorded at 60 minutes after processing as the

lipid sample was found to be too soft to measure its hardness at this time.

Results and discussion

One of the fundamental unknowns related to the effects of ultrasound on any system, is the population of bubbles present within the media. This is key as the interaction of these bubbles with the sound field drives many of the physical and chemical processes that occur. To characterise this population and see how this changed over time and with the type of cavitation environment present, an optical transmission sensor was deployed (see ref. 19 for further details). Here, the response of a simple photodiode was monitored as a function of time and used to estimate the size and number of the bubbles present in the media as the oil is drawn through a capillary.

In these experiments the population of bubbles within the media was followed as a function of time over a ~300 s time window after the exposure of the liquid to HIU was terminated. This is limited by the crystallisation of the media. Fig. 1 shows the results of these experiments for an APS sample exposed to different cavitation environments (specifically different cluster types generated by applying different HIU power levels to the sample). Fig. 1(a), for example, shows the response for the bifurcated streamer (BiS) generated under these conditions. In this case the smallest size range was observed. Note, the sensor and analysis used limits the lower detectable radius to the order of 45 μm. Hence, bubbles smaller that this will not be detected. This is particularly relevant to the BiS event as this appears to produce a mist of small bubbles. Fig. 1 also shows that as the power of the HIU source was increased the number and size of the detectable bubbles within the fluid increased. Fig. 2 shows how the number of events (determined as detectable transients above the baseline) within the media changed as the cluster type and the temperature of the APS sample were altered. It is also important to note that these measurements were performed after the HIU source had been terminated. This indicates that the bubble population is long lived and of varied size.

Turning to the lifetime of the events within the media, Fig. 2 shows how this varies with both the temperature and the HIU power (and type of cluster dynamics generated). Fig. 2 shows that the number of events rises with HIU power and the bubble retention time (defined as the time when transients above the baseline could be recorded) climbs as the HIU power was increased. The temperature of the media also has an effect. For example, Fig. 2(a) shows that the numbers of bubbles recorded are higher at lower temperatures while the retention time was generally smaller at higher temperature. This observation is presumably a result of differing generation conditions and retention effects within the lipid. The decreased viscosity of the lipid at higher temperature is expected to allow bubbles, particularly large ones in the population, to be lost through buoyancy effects over the time course of the experiment. For example, in APS the terminal velocity[21–24] of a bubble with a

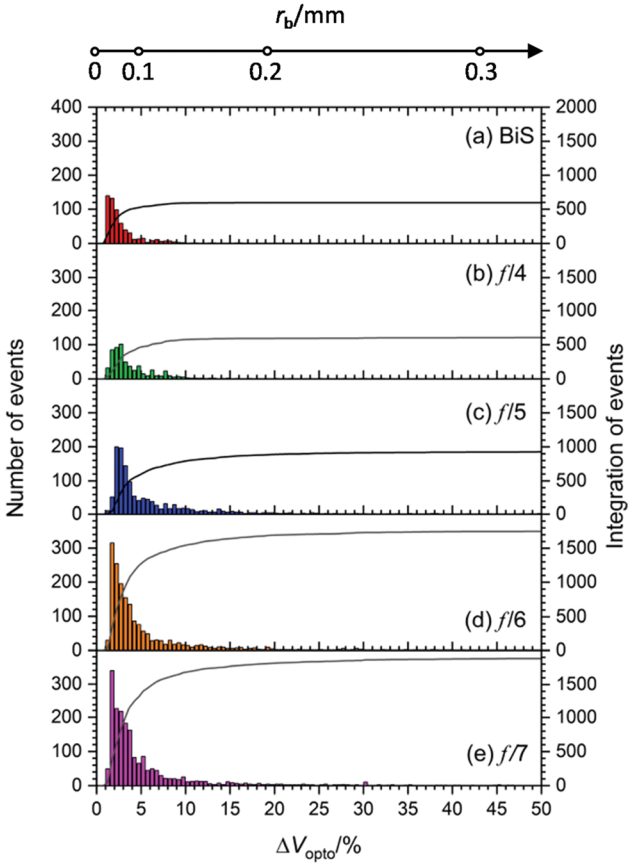

Fig. 1 Plots showing stacked histograms of the change in the optical sensor voltage signal as a percentage (ΔV_{opto}/%) calculated from the bubble translocation events recorded within all-purpose shortening after HIU treatment at different power levels. HIU was applied for 10 seconds at (a) 10 W (■), (b) 18 W (■), (c) 36 W (■), (d) 51 W (■) and (e) 75 W (■) power level. Events were analysed for 300 seconds after HIU was terminated. The cluster type is indicated. The pressure differential was −113 mbar and the sample temperature was 26.1 °C. The bin width for each plot was 0.25%. The integration of events within each distribution is given by black line (right axis, —). The upper scale bar represents the estimated bubble diameter.

radius of 100 μm can be calculated to be ~0.91 mm s^{-1} at 30 °C while it is ~0.64 mm s^{-1} at 20 °C (see SI data, Fig. S3, ESI†). In turn the smaller the bubble, the slower its rise time (see SI data, Fig. S2, ESI†). This implies that small bubbles produced in a lipid are slow moving over the timeframe of these experiments. However, other effects are worth consideration. For example, dissolution of bubbles in a gas saturated media is driven by a number of effects including the Ostwald coefficient[25] of the gas in question, the diffusion coefficient of the gas in the media and the surface tension[26] of the gas/liquid interface. Epstein and Plesset reported that the dissolution time under these conditions can be calculated.[27] If we compare a bubble with a radius of 10 μm in water and oil, the dissolution times are significantly different (see SI data, Fig. S4, ESI†). For example, in water this can be calculated as 7.59 s while in oil the same sized bubble will have a dissolution lifetime of 168 s. This longer lifetime (which may be extended through shell effects[28]

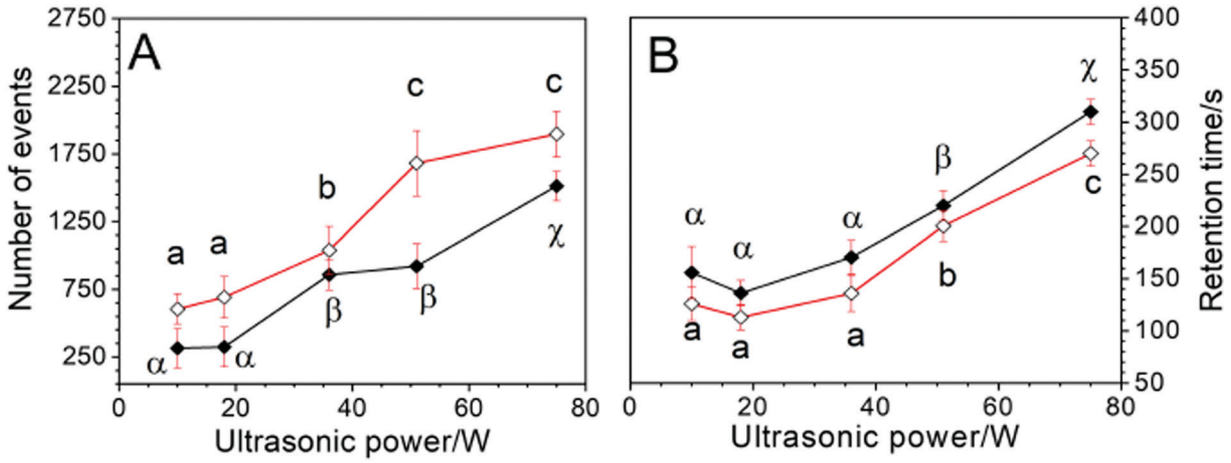

Fig. 2 Plots depicting the average number of detectable bubble events (A) and the retention time (B) of gas bubble species recorded with the opto-counter device after HIU treatment within all-purpose shortening as a function of the ultrasonic power applied. These attributes were compared as a function of ultrasonic power at 26 °C (◊); and 30 °C (◆). Mean values are plotted with 95% confidence levels, recorded over three replicate experiments for each condition. The opto-counter was positioned centrally at the base of the cell. The PLE was secured 5 mm above the opto-counter surface with a horizontal displacement of 2 mm from the channel opening. HIU was applied for a 10 sec duration in each case and the pressure differential applied across the opto-counter channel was −113 mbar. Data points labelled with different lower-case letters (a, b *etc.*) are statistically different ($p \leq 0.05$) at 26 °C. Data points labelled with different Greek letters (α, β *etc.*) are statistically different at 30 °C.

in the crystallising media) of these particularly small bubbles suggests that cluster environments that produce these (*e.g.*, the BiS system) may be more efficient in terms of primary nucleation processes in these lipid environments.

If the bubble population alone is the important factor, the results contained in Fig. 2 suggest that the $f/4$ cluster should behave very similarly to the BiS system. However, for the BiS event (produced at the lowest power, 10 W) an unusually high crystallisation rate was observed. This suggests that there may be other effects that come into play. In order to probe these effects, a series of experiments were performed. In the first set, the cluster was isolated from the crystallising media to separate the cluster and its bubble population from the main crystallising media. In the second set of experiments, the time of HIU application and the effect of added crystals were investigated.

To isolate the cluster/HIU tip from the crystallising media a dual compartment cell was utilised. Fig. 3 shows a schematic representation of the cell employed. This cell had two compartments. The PLE, cluster and associated bubbles were contained in the upper compartment. This contained sunflower oil. The lower, main chamber contained the APS sample. Fig. 4 shows the response of the hydrophone as the conditions were altered. In the absence of the upper containment chamber, Fig. 4 shows a typical response for the effect of HIU on a crystallising APS sample. The amplitude of the signal (—) falls with time. Fig. 4 also shows the effect of the upper chamber and the materials that are deployed. If the walls of the upper chamber are all 3 mm acrylic, the signal detected by the hydrophone (—) is severely reduced in comparison to the chamber free example. This indicates that as well as containing the bubble population and cluster in the upper chamber, sound propagation into the APS sample is severely restricted. However, if the base of the containment cell is changed to 0.3 mm ABS, the signal recorded

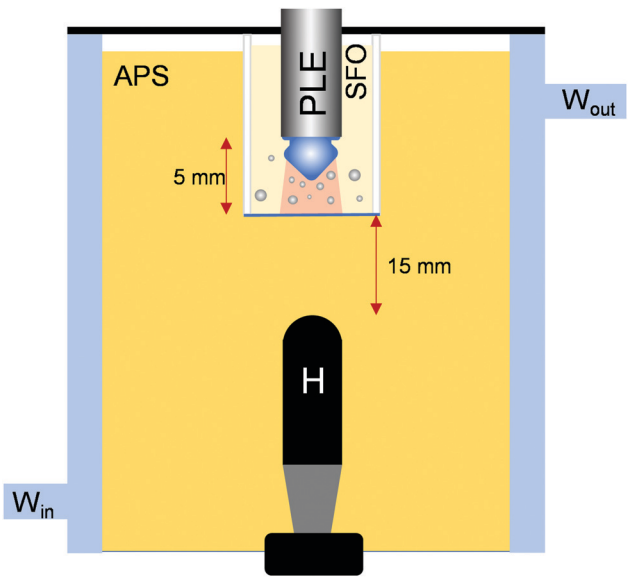

Fig. 3 Schematic representation of the containment cell experimental setup. Here a piston like emitter (PLE) acts as the source for HIU. Under the conditions employed a cluster was formed at the surface of the probe (▮). Gas bubbles originating in this zone (▮) are contained in the upper compartment which contained sunflower oil (SFO). The base of the containment cell was be altered from acrylic (3 mm) to ABS (0.3 mm). The main chamber contained the hydrophone (H) immersed in APS. The separation between the tip of the PLE and the base of the containment cell and the base of the containment cell and the hydrophone are included. The whole system was jacketed with water to maintain temperature control on the system.

by the hydrophone (—) is significantly higher. This change in behaviour is likely to be as a result of the material characteristics including the acoustic impedance of the materials involved and their relative attenuation effects. For example,

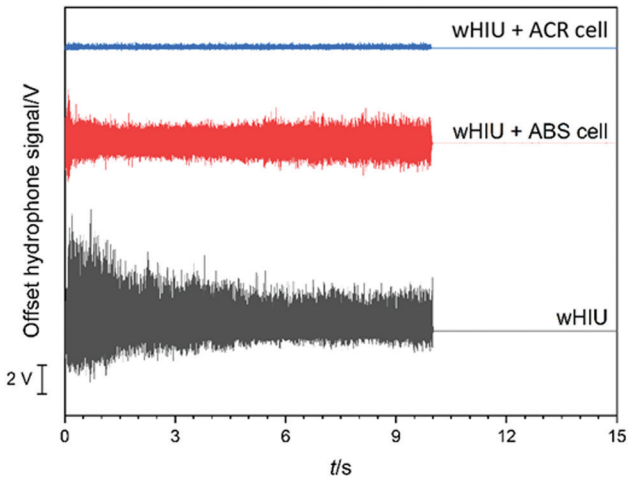

Fig. 4 Plots showing the hydrophone time series recorded at 30 °C during a 10 s HIU exposure and a further 5 s after the cavitation period. HIU was applied at 75 W (*f*/7) with acrylic (ACR) (—) and ABS plastic (—) base materials. The hydrophone signal in the absence of the inner chamber (—) is also given for comparison. The scale bar represents 2 V hydrophone signal for comparison.

the acoustic impedance of ACR is higher than ABS which would suggest more sound energy was reflected from the lipid/ACR interface. In addition, the attenuation coefficient of ABS is $\sim$11 dB cm^{-1} *vs.* $\sim$12.4 dB cm^{-1} for ACR.[29] These properties, in addition to the change of thickness of the samples, will contribute significantly to the observed change in sound transmission into the lower chamber. The effect on the crystallisation kinetics of the APS sample was also assessed under these conditions. Table 1 shows how the conditions employed affected the process.

These results were obtained from analysing the solid fat content as a function of time over a 60 minutes period using a pNMR approach. The results in Table 1 show that, while we restrict the cluster and bubble population to the upper chamber, transmission of sound to the APS has an effect on the crystallisation kinetics with the degree of transmission affecting the enhancement observed. First, the ABS cell gave a greater enhancement compared to the acrylic case and the without HIU (woHIU) controls in agreement with the sonic transmission data shown in Fig. 4. Second, and significantly, the isolation of the bubble population from the main APS chamber did not

Table 1 Table showing the maximum solid fat content (a_G), maximal crystal growth rate (μmax) and induction time for crystallisation (λ) calculated from fitting SFC *vs.* time curves to the Gompertz model. Values are recorded from three repeat crystallisation experiments and expressed as mean ± 95% CL to 1 s.f. Values labelled with different subscripts indicate significant differences ($p \leq 0.05$)

Conditions	a_G (%)	μ_{max} (% min^{-1})	λ (min)
wHIU – no inner cell	$7.7 \pm 0.3^{a,b}$	0.63 ± 0.02^{c}	14.2 ± 0.6^{b}
wHIU – ACR inner cell	$8.0 \pm 0.4^{a,b}$	0.30 ± 0.03^{a}	27.1 ± 0.9^{a}
wHIU – ABS inner cell	8.1 ± 0.1^{a}	0.43 ± 0.05^{b}	27.0 ± 0.5^{a}
woHIU – ABS inner cell	8.2 ± 0.2^{a}	0.27 ± 0.01^{a}	28.4 ± 0.7^{a}
woHIU – no inner cell	7.3 ± 0.5^{b}	0.29 ± 0.04^{a}	29 ± 1^{a}

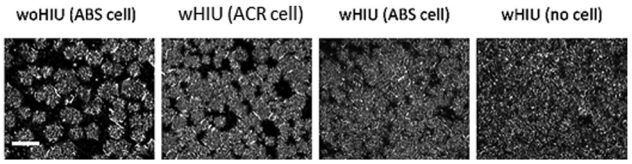

Fig. 5 Polarised light microscopy (PLM) images of APS obtained after 60 min of crystallisation at 30 °C with HIU using an inner cell with a base comprised of acrylic, ACR, and ABS. PLM images recorded in the absence of HIU with the inner cell and in the presence of HIU without the inner cell are given for comparison. The white scale bar in first image represents 100 μm.

completely remove the enhanced crystallisation kinetics observed. This suggests that the progress of the shock like emission into the sample had an effect. This is presumably linked to the action of this physical effect on the crystallites within the media. Third, this physical effect is supported by observing the changes in the crystal structure of the resultant material. Fig. 5 shows the microstructure of samples taken under the various conditions explored.

Fig. 5 shows that the microstructure of the sample changes from the control woHIU towards the wHIU (no isolation cell) as expected from the kinetics data reported in Table 1. These results suggest that a clear effect of ultrasound is associated with the progression of the sound waves through the media. It is postulated here that the intense 'shock like' emissions which are associated with the cluster collapse at the PLE tip cause fragmentation of the pre-existing crystals in the sample and lead to secondary nucleation effects. To support this, a set of experiments were performed to investigate the effect of the presence of pre-existing nuclei on the process. Fig. 6 shows the acoustic data gathered from samples cooled to a set temperature and then exposed to ultrasound. However, the delay

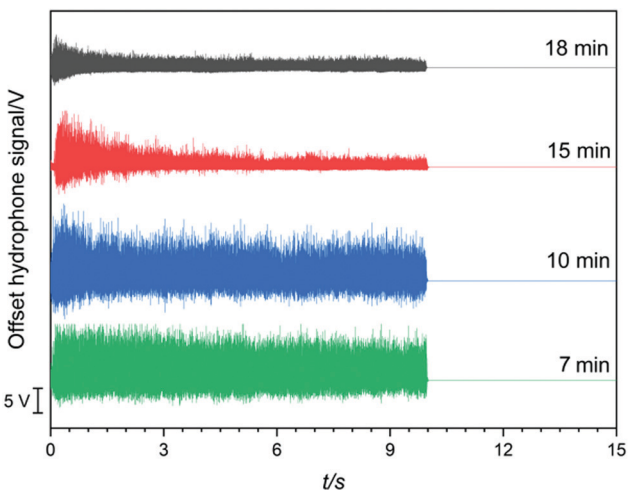

Fig. 6 Plot showing the hydrophone time series of APS crystallised at 30 °C during a 10 s HIU pulse duration and a further 5 s after the cavitation period. HIU was applied at 75 W (*f*/7 cluster) ultrasonic power at 7 (—), 10 (—), 15 (—) and 18 (—) minutes after the sample reached 30 °C. Scale bar represents 5 V hydrophone signal for comparison.

Table 2 Table showing the apparent second order constant (k_2) obtained from fitting the decay of the hydrophone envelope signal to a second order model. High-intensity ultrasound was applied at 75 W (*f*/7) power level over a 10 s period. All samples were cooled to 30 °C with the indicated time stating the period between the APS sample entering the cell and the application of HIU. These values are recorded from three repeat experiments and expressed as mean ±95% CL to 1 s.f. Values labelled with different subscripts indicate significant differences ($p \leq 0.05$)

t cooling to 30 °C min^{-1}	k_2/V^{-1} s^{-1}	r^2
7	0.03 ± 0.03^{a}	0.95
10	0.13 ± 0.05^{b}	0.97
15	0.28 ± 0.02^{c}	0.97
18	0.31 ± 0.02^{c}	0.97

between the sample reaching the desired crystallisation temperature (here 30 °C) and the application of HIU was varied.

Fig. 6 shows that as the time period resting at 30 °C was increased (see Fig. S1, ESI† for cooling profile), the attenuation rate of the acoustic signal detected by the hydrophone increased.

The effective attenuation coefficient of the crystallising media (see ref. 18 for details) was calculated by fitting the hydrophone positive envelope to a second order model. Table 2 shows how the attenuation coefficient changes in response to the time at which HIU was applied to the sample. The data suggests that the attenuation of the hydrophone signal depends strongly on the time period spent at the crystallisation temperature. In turn, this indicates that the attenuation of the signal is largely in response to the interaction of the HIU with the crystal population. As a result, little attenuation was observed for the data recorded at 7 minutes. This is unsurprising as the temperature of the sample was ~35 °C at this point. Under these conditions no crystals are expected and the attenuation coefficient, which appears strongly linked to the crystal population, is close to zero. However, as the sample temperature was reduced further, a greater crystal population (which has been associated with an increased effectiveness of HIU[30–32]) and hence acoustic attenuation was observed.

Turning to the kinetics of crystallisation, Table 3 shows how the different conditions affect the rates observed. These results indicate that all periods tested showed faster crystallisation kinetics than the control. Critically the measurements at 7 minutes where the sample was ~35 °C, shows a significant improvement in the rate of crystallisation (μ_{max}) and a reduction in the induction time (λ). This shows that in the absence of observable crystals, HIU has a positive effect on the kinetics.[30–32] This presumably indicates that the bubble population is able to contribute to primary nucleation of the sample. This is supported by the lifetime measurements shown in Fig. 2 which showed that detectable bubbles last for at least 300 s (and smaller bubbles will be longer lasting in comparison). This agrees with the buoyancy and dissolution effects previously discussed. Hence the bubble population generated at 7 mins will last into the time period when crystallization occurs. This supports the primary nucleation effect within the sample. However, as the time period before the application of HIU was increased, significant attenuation of the hydrophone signal was observed (see Table 2) and a greater acceleration in the crystallisation kinetics was seen (see Table 3). This observation suggests that HIU has a significant secondary nucleation effect whereby crystals are fragmented by the conditions present (either shear effects around oscillating bubbles present or the large pressure shocks generated by the cluster collapses, supported by the results shown in Table 1).

In order to probe these conditions further, polarised light imaging of samples after different sets of conditions at the point of HIU application and after 60 minutes was undertaken. Fig. 7 shows the images obtained. These images show that no observable crystals are present at 7 min (T_m) in agreement with the acoustic attenuation data shown in Fig. 6. Fig. 7 also shows the changes in the microstructure of the sample after 60 mins was similar to the woHIU control. However, the enhanced kinetics observed at this point suggest that the primary (bubble induced) crystallisation rate does not have a marked effect on the resultant microstructure. This observation suggests that

Table 3 Table showing the maximum solid fat content (a_G), maximal crystal growth rate (μ_{max}) and induction time for crystallisation (λ) calculated from fitting SFC *vs.* time curves to the Gompertz model. Values are recorded from three repeat crystallisation experiments and expressed as mean ± 95% CL to 1 s.f. The numbers in parenthesis show the sample temperature. Values labelled with different subscripts indicate significant differences ($p \leq 0.05$)

Conditions [temp/°C]	a_G (%)	μ_{max} (% min^{-1})	λ (min)
woHIU	7.3 ± 0.5^{a}	0.29 ± 0.04^{a}	29 ± 1^{a}
wHIU 7 min [35]	7.6 ± 0.1^{b}	0.49 ± 0.03^{b}	21.5 ± 0.3^{b}
wHIU 10 min [30]	7.7 ± 0.1^{b}	0.52 ± 0.06^{b}	18.8 ± 0.3^{c}
woHIU 15 min [30]	7.7 ± 0.3^{b}	0.63 ± 0.02^{c}	14.2 ± 0.6^{d}
woHIU 18 min [30]	7.6 ± 0.4^{b}	0.76 ± 0.08^{d}	14.5 ± 0.9^{d}

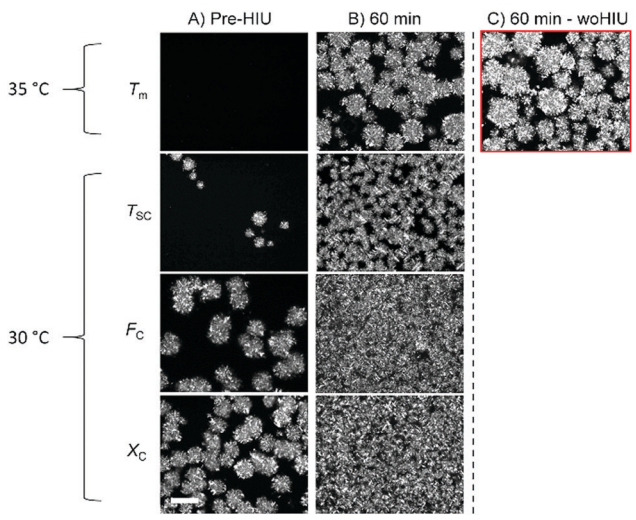

Fig. 7 PLM images showing the crystal microstructure of APS samples obtained (A) immediately before the HIU treatment (75 W, *f*/7, 10 s) was applied at 7 min (T_m), 10 min (T_{SC}), 15 min (F_C) and 18 min (X_C), (B) after 60 min of crystallisation at 30 °C for each of these treatment conditions and (C) a control experiment showing the microstructure of a sample held at 30 °C 60 min crystallisation without (wo) HIU treatment. Scale bar represents 100 μm.

primary nucleation occurs in both the treated and untreated samples in a similar way as expected. However, as the crystal population increased (see Fig. 7, panel 'A', T_{SC}, F_C and X_C), crystals are observed prior to the application of ultrasound. The size and number of crystals is also seen to increase as the cooling period was increased. The application of ultrasound (see Fig. 7 panel 'B' for the structure after 60 minutes) shows that these crystals are broken up significantly with the average crystal size reducing visibly while the packing density seems to be greater for those samples held for longer at 30 °C before the application of ultrasound (10 s, 75 W in all cases) to the system. Hence, the more delayed the application of ultrasound (and the generation of a significant crystal population) yields significant secondary[30] nucleation effects further enhancing the crystallisation kinetics (see Table 3) and altering the microstructure (see Fig. 7).

It could be envisaged that this change in microstructure in response to HIU (and enhanced secondary nucleation combined with primary nucleation effects) can alter the material properties of the resultant material. Fig. 8 shows how the material characteristics are affected by these effects. First, the elastic modulus is the same for the control (wo) and 7 minute experiment. However, where secondary effects are expected (when there is a significant crystal population when the sample was exposed to ultrasound), the elastic modulus increases significantly and continues to increase as the pre-HIU crystal population increases. Second, there is an increase in the hardness of all samples when exposed to HIU which increases further as the cooling time was extended. This presumably indicates that any increase in the kinetics (both primary and secondary) affects this parameter.

The evidence presented suggests that both primary and secondary effects are triggered by the application of HIU to the APS samples with the exact combination dictated by the crystal population within the sample at the point of HIU application. To test this assertion further, a set of experiments were performed where APS crystals were added to the media (by the addition of a small quantity of APS allowed to crystallise in the absence of HIU for 25 minutes) and the effect of this addition was investigated. Table 4 shows the effect of these additions. The addition of crystals with stirring or HIU display a greater rate than HIU alone. This suggests that the crystal population and the mechanical agitation of this media plays a significant role in the enhancement of the crystallisation kinetics.[33,34] The material characteristics of the samples also showed some variation. However, the HIU treated samples showed the greatest change in agreement with the similarity of the PLM images of these samples (see SI Fig. S5 and S6, ESI† respectively).

Turning to the effect of stirring the sample (and the induced shear, which has been shown to be effective at accelerating crystallisation of IESBO[34]), a set of experiments were performed to probe this effect. Table 5 shows the results of this investigation. These results indicated that mild stirring (200 rpm) was not effective in enhancing the crystallisation process while higher rates (600 rpm) showed a significant increase.

This suggests that mechanical agitation, if of sufficient intensity, is effective at accelerating the crystallisation process. Interestingly, the velocity of the stirrer tips for 600 rpm can be estimated at $\sim$0.6 m s^{-1}. This is slightly lower than the streamer velocity produced by the cluster.[16] However, the rates of crystallisation are far lower than for the HIU case suggesting

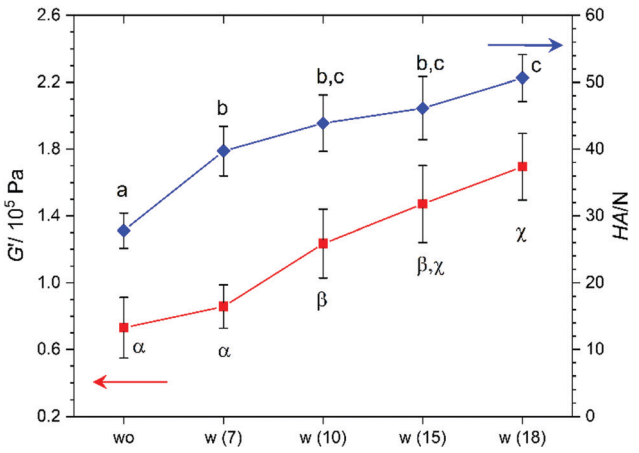

Fig. 8 Plot showing the elastic modulus (G', ■) and hardness (HA, ◆) measurements for APS crystallised at 30 °C with (w) and without (wo) HIU treatment at 75 W. HIU was applied at 7, 10, 15 and 18 min after initial sample cooling. Values are recorded from three repeat crystallisation experiments and expressed as mean ± 95% CL. Values labelled with different superscript lettering indicate significant differences ($p \leq 0.05$). The numbers in parenthesis on the x axis represent the time period at which HIU was applied (minutes).

Table 4 Table showing the maximum solid fat content (a_G), maximal crystal growth rate (μ_{max}) and induction time for crystallisation (λ) calculated from fitting SFC *vs.* time curves the Gompertz model. Values are recorded from three repeat crystallisation experiments and expressed as mean ± 5% CL to 1 s.f. All treatments were for 10 s at 15 minutes into the cooling period. Values labelled with different subscripts indicate significant differences ($p \leq 0.05$)

Conditions	a_G (%)	μ_{max} (% min^{-1})	λ (min)
woHIU	7.3 ± 0.5^a	0.29 ± 0.04^a	29 ± 1^a
10 cm^3 crystal addition, 200 rpm	7.8 ± 0.1^b	0.77 ± 0.03^b	18.4 ± 0.3^b
10 cm^3 crystal addition, wHIU	7.6 ± 0.2^b	0.72 ± 0.05^b	14.3 ± 0.4^c
wHIU	7.7 ± 0.4^b	0.63 ± 0.08^c	14.2 ± 0.6^c

Table 5 Table showing the maximum solid fat content (a_G), maximal crystal growth rate (μ_{max}) and induction time for crystallisation (λ) calculated from fitting SFC *vs.* time curves the Gompertz model. Values are recorded from three repeat crystallisation experiments and expressed as mean ± 95% CL to 1 s.f. All treatments were for 10 s at 15 minutes into the cooling period. Values labelled with different subscripts indicate significant differences ($p \leq 0.05$)

Conditions	a_G (%)	μ_{max} (% min^{-1})	λ (min)
woHIU	7.3 ± 0.5^a	0.29 ± 0.04^a	29 ± 1^a
200 rpm	8.1 ± 0.2^b	0.33 ± 0.04^a	29 ± 2^a
600 rpm	7.9 ± 0.3^b	0.42 ± 0.06^b	23 ± 2^b
wHIU	7.7 ± 0.3^b	0.63 ± 0.02^c	14.2 ± 0.6^c

that it is not only the flow but the other physical effects of the cluster (shocks, local shear *etc.*) which need to be considered.

The results presented here all suggest that the effect of ultrasound on fat crystallisation is multifaceted. The cavitation environment can generate primary nucleation sites through the production of a significant long lived bubble population. In turn the action of the cluster, which produces a strong and regular shock like emission, further accelerate the crystallisation kinetics through, presumably, secondary nucleation effects. At this point some regard to the structure and nature of the APS sample should be noted.

It has been shown that crystal fragmentation[35–37] can be generated in a variety of systems and this process is related to the mechanical properties of the sample. For example, Kim *et al.* showed that salt crystals could be fragmented in an ultrasonic field with the rate of fragmentation related to the Vickers hardness and Youngs modulus of the material employed.[36] If we consider APS in comparison, it is interesting to note that the crystals[38,39] (or spherulites) are really conglomerates of smaller TAG nanocrystals held together by weak van der Waals forces.[39] Correspondingly, the Youngs modulus[38] of a single spherulite is nearly 10^5 smaller[38] at $\sim$1 MPa compared to a material like NaF (77.5 GPa), for example. Hence, we can expect that such APS spherulites will be fragmented easily in comparison by the forces generated by the HIU treatment of the sample. This agrees with the observation in the data provided above. However, further insight is possible. The bifurcated streamer (BiS) system which can be generated in these oil systems was shown[18] to be highly active in the acceleration of APS crystallisation, in excess of what would be expected on a power basis alone (compared to other clusters). The reasons for this are now, perhaps, more apparent.

The BiS system possess two of the key components that have been shown to enhance APS crystallisation. First, it generates a set of small gas bubbles which populate the fluid. Thus, this dual streamer could be expected to enhance primary nucleation events in excess of a single cluster stream. Second, the strong pulse like shock generated by the cluster collapse (the strongest globally measurable emission in the system) is more frequent in comparison to all other clusters. Indeed, the BiS's anatomy consists of two clusters oscillating at an $f/2$ period but 180° out of phase with one another. This essentially results in a shock emission into the sample at f, the ultrasonic source, (and hence a weak emission). The fluid, bubble population and crystals are hence exposed to a pressure shock every cycle of the source which is more often than any other cluster environment measured for these oil clusters. The shear forces around the clusters themselves may also play a role, as yet to be quantified. However, the BiS event has two clusters so may also be at an advantage here. Finally, the bubbles within the media will also be an active part of the system with their motion, presumably classed as non-inertial cavitation, in the associated sound field

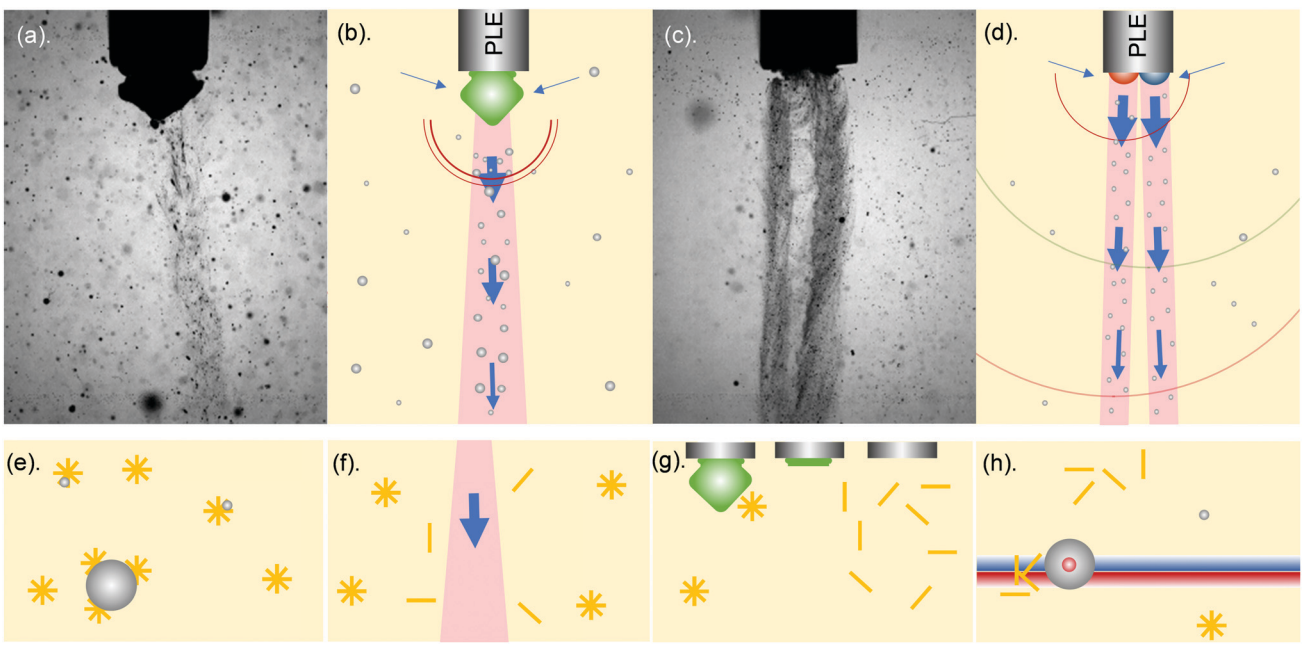

Fig. 9 Images and schematic representations of the processes and mechanism present. (a) shows the piston like emitter (PLE, 3.2 mm diameter), arrowhead cluster, streamer and bubble population in sunflower oil. (b) shows the heater streamer (▭), shock emission (—), bubbles and fluid flow (→). Here the size of the arrow indicates the velocity magnitude. Liquid is drawn in close to the cluster and driven out in the streamer formed below the cluster. (c) shows the BiS event with the two clusters (▭, ▭) on the tip of the PLE and the dual streamer structure. (d) shows the clusters with different colours indicating the phase difference between the two. Shows are also coloured (—, —) to indicate the alternating origin between the two clusters at the PLE tip. (e) shows the bubble population and primary nucleation sites on the gas/liquid interface. (f) shows the shear around the streamer causing spherulite breakup. (g) shows the collapse of the cluster at the PLE and the shear induced breakup of the local spherulites. (h) shows the shock progression through the liquid and either spherulite breakup as a result of the shock or through its action on the bubble population through local shear, for example. Note the schematics are not drawn to scale and for illustration of the processes present.

will produce local shear[40] through their motion and the associated microstreaming.[7] Hence, these events will contribute to the secondary nucleation effects. Fig. 9 brings the observed components together and highlights the proposed important factors and the characteristic of each environment.

Finally, the contribution of the relative shear of the differing components, whether that is the fluid driven in the streamer, the motions around the cluster itself or the motion of gas bubbles in response to the streamer or the shock emission into the bulk, all need to be assessed and quantified. This remains a fascinating question in relation to the relative effects of the physical processes within the crystallising media.

Conclusions

A number of factors have been explored. The evidence suggests that both primary and secondary nucleation is important in assessing the acceleration of crystallisation of APS as a result of HIU action. However, this effect is clearly multifaceted with contributions from more than one origin likely. To this end the abnormally high rate of crystallisation in the presence of the BiS event can now be further understood through its unusual characteristics. Specifically, this system produces many small bubbles (and hence can be an effective primary nucleation source) and exposes the fluid to more frequent pressure shocks which accelerate secondary nucleation effects.

Conflicts of interest

There are no conflicts to declare.

Acknowledgements

This project was supported by Agriculture and Food Research Initiative (AFRI) Grant No. 2017-67017-26476 from the USDA National Institute of Food and Agriculture, Improving Food Quality-A1361. This paper was approved by the Utah Agricultural Experiment Station as Paper Number 9545.

References

1 K. S. Suslick, D. A. Hammerton and R. E. Cline, The sonochemical hotspot, *J. Am. Chem. Soc.*, 1986, **108**, 5641–5642.
2 K. S. Suslick, Sonochemistry, *Science*, 1990, **247**, 1439–1445.
3 K. S. Suslick, S. J. Doktycz and E. B. Flint, On the origin of sonoluminescence and sonochemistry, *Ultrasonics*, 1990, **28**, 280.
4 J. N. Brantley, K. M. Wiggins and C. W. Bielawski, Polymer mechanochemistry: The design and study of mechanophores, *Polym. Int.*, 2013, **62**, 2–12.
5 P. R. Birkin, R. O'Connor, C. Rapple and S. S. Martinez, Electrochemical measurement of erosion from individual cavitation events generated from continuous ultrasound, *J. Chem. Soc., Faraday Trans.*, 1998, **94**, 3365–3371.
6 Y. E. Watson, P. R. Birkin and T. G. Leighton, Electrochemical detection of bubble oscillation, *Ultrason. Sonochem.*, 2003, **10**, 65–69.
7 S. A. Elder, Cavitation microstreaming, *J. Acoust. Soc. Am.*, 1958, **31**, 54.
8 F. R. Young, *Cavitation*, Imperial College Press, London, 1999.
9 L. A. Crum and G. T. Reynolds, Sonoluminescence produced by 'stable' cavitation, *J. Acoust. Soc. Am.*, 1985, **78**, 137–139.
10 A. J. Walton and G. T. Reynolds, Sonoluminescence, *Adv. Phys.*, 1984, **33**, 595–660.
11 S. Martini, R. Tejeda-Pichardo, Y. Ye, S. G. Padilla, F. K. Shen and T. Doyle, Bubble and crystal formation in lipid systems during high-intensity insonation, *J. Am. Oil Chem. Soc.*, 2012, **89**, 1921–1928.
12 S. Martini, in *Sonocrystallization of Fats*, Springer International Publishing, New York, 2013, pp. 41–62.
13 A. H. Suzuki, J. Lee, S. G. Padilla, S. Martini, A. H. Suzuki, J. Lee and S. G. Padilla, Altering functional properties of fats using power ultrasound, *J. Food Sci.*, 2010, **75**, E208–E214.
14 Acumen Research and Consulting (accessed 22/09/2021).
15 M. E. Abdelsalam and P. R. Birkin, A study investigating the sonoelectrochemical degradation of an organic compound employing Fenton's reagent, *Phys. Chem. Chem. Phys.*, 2002, **4**, 5340–5345.
16 P. R. Birkin, T. M. Foley, T. T. Truscott, A. Merritt and S. Martini, Cavitation clusters in lipid systems – surface effects, local heating, outgassing and streamer formation, *Phys. Chem. Chem. Phys.*, 2017, **19**, 6785–6791.
17 I. Foubert, K. Dewettinck and P. A. Vanrolleghem, Modelling of the crystallization kinetics of fats, *Trends Food Sci. Technol.*, 2003, **14**, 79–92.
18 J. J. Youngs, P. R. Birkin, J. Lee, T. T. Truscott and S. Martini, Enhanced crystallisation kinetics of edible lipids through the action of a bifurcated streamer, *Analyst*, 2021, **146**, 4883–4894.
19 P. R. Birkin, J. J. Youngs, T. T. Truscott and S. Martini, Development of an optical flow through detector for bubbles, crystals and particles in oils, *Phys. Chem. Chem. Phys.*, 2022, **24**, 1544–1552.
20 P. R. Birkin, S. Linfield, G. Denuault, R. Jones, J. J. Youngs and E. Wain, An analytical differential resistance pulse system relying on a time shift signal analysis-applications in coulter counting, *ACS Sens.*, 2019, **4**, 2190–2195.
21 R. Clift, J. R. Grace and M. E. Weber, *Bubbles, Drops, and Particles*, Dover Publications Inc., New York, 2005.
22 N. P. Brandon and G. H. Kelsall, Growth kinetics of bubbles electrogenerated at microelectrodes, *J. Appl. Electrochem.*, 1985, **15**, 475–484.
23 N. P. Brandon, *The growth kinetics and interfacial properties of electrogenerated bubbles*, PhD thesis, Imperial College, 1985.
24 G. H. Kelsall, S. Tang, A. L. Smith and S. Yurdakul, Measurement of rise and electrophoretic velocities of gas bubbles, *J. Chem. Soc., Faraday Trans.*, 1996, **92**, 3879.
25 R. Battino, T. R. Rettich and T. Tominaga, The solubility of nitrogen and air in liquids, *J. Phys. Chem. Ref. Data*, 1984, **13**, 563.

26 W. Duangsuwan and U. Tuzun, The dynamics of single air bubbles and alcohol drops in sunflower oil at various temperatures, *AIChE J.*, 2011, **57**, 897–910.
27 P. S. Epstein and M. S. Plesset, On the Stability of Gas Bubbles in Liquid-Gas Solutions, *J. Phys. Chem.*, 1950, **18**, 1505–1509.
28 M. A. Borden and M. L. Longo, Dissolution behavior of lipid monolayer-coated, air-filled microbubbles: Effect of lipid hydrophobic chain length, *Langmuir*, 2002, **18**, 9225–9233.
29 Onda, Acoustic Properties of Plastics, 2003.
30 Y. Ye, A. Wagh and S. Martini, Using high intensity ultrasound as a tool to change the functional properties of interesterified soybean oil, *J. Agric. Food Chem.*, 2011, **59**, 10712.
31 A. H. Suzuki, J. Lee, S. G. Padilla and S. Martini, Altering functional properties of fats using power ultrasound, *J. Food Sci.*, 2010, **75**, E208–14.
32 S. Martini, A. H. Suzuki and R. W. Hartel, Effect of high intensity ultrasound on crystallization behavior of anhydrous milk fat, *J. Am. Oil Chem. Soc.*, 2008, **85**, 621–628.
33 J. V. Kadamne and S. Martini, Sonocrystallization of interesterified soybean oil with and without agitation, *J. Am. Oil Chem. Soc.*, 2018, **95**, 571–582.
34 R. C. Silva, J. Lee, V. Gibon and S. Martini, Effects of high intensity ultrasound frequency and high-speed agitation on fat crystallization, *J. Am. Oil Chem. Soc.*, 2017, **94**, 1063–1076.
35 B. W. Zeiger and K. Suslick, Sonofragmentation of molecular crystals: Observations and modeling, *Proc. Meet. Acoust.*, 2013, **19**, 14530–14533.
36 H. N. Kim and K. S. Suslick, Sonofragmentation of ionic crystals, *Chem. – Eur. J.*, 2017, **23**, 2778–2782.
37 J. R. G. Sander, B. W. Zeiger and K. S. Suslick, Sonocrystallization and sonofragmentation, *Ultrason. Sonochem.*, 2014, **21**, 1908–1915.
38 H. Y. Yoshikawa, D. A. Pink, N. C. Acevedo, F. Peyronel, A. G. Marangoni and M. Tanaka, Mechanical response of single triacylglycerol spherulites by using microcolloidal probes, *Chem. Lett.*, 2017, **46**, 599–601.
39 N. C. Acevedo, F. Peyronel and A. G. Marangoni, Nanoscale structure intercrystalline interactions in fat crystal networks, *Curr. Opin. Colloid Interface Sci.*, 2011, **16**, 374–383.
40 J. A. Rooney, Hemolysis near an ultrasonically pulsating bubble, *Science*, 1970, **169**, 869–871.